Available online at www.sciencedirect.com
SCIENCE DIRECT®
Communications in Nonlinear Science and Numerical Simulation 8 (2003) 375–387
Communications in Nonlinear Science and Numerical Simulation
www.elsevier.com/locate/cnsns

Clustering and ensembles inequivalence in the ϕ^4 and ϕ^6 mean-field Hamiltonian models

Thierry Dauxois [a], Stefano Lepri [a,b], Stefano Ruffo [a,b,*,1]

[a] *Laboratoire de Physique, UMR-CNRS 5672, ENS Lyon, 46 Allée d'Italie, 69364 Lyon cédex 07, France*
[b] *Dipartimento di Energetica, Università di Firenze INFM and INFM, 'via S. Marta, 3, 50139 Firenze, Italy*

Abstract

We investigate a model of globally coupled conservative oscillators. Two different algebraic potentials are considered that display in the canonical ensemble either a second (ϕ^4) or both a second and a first-order phase transition separated by tricritical points (ϕ^6). The stability of highly clustered states appearing in the low temperature/energy region is studied both analytically and numerically for the ϕ^4-model. Moreover, long-lived out-of-equilibrium states appear close to the second-order phase transition when starting with "water-bag" initial conditions, in analogy with what has been found for the Hamiltonian mean-field model. The microcanonical simulations of the ϕ^6-model show strong hysteretic effects and metastability near the first-order phase transition and a narrow region of negative specific heat.

PACS: 05.20.–y; 05.45.–a
Keywords: Long-range interaction; Coherent structures; Mean-field; Microcanonical ensemble

1. Introduction

The treatment of long-range interacting systems remains a challenging issue in thermodynamics and statistical mechanics [1]. Serious theoretical difficulties arise because internal energy, entropy and other thermodynamic quantities are no longer additive, i.e. a part of a system has not the same thermodynamic properties of the whole. This originates unusual effects, like negative specific heat and the inequivalence of statistical ensembles even in the limit of infinite number of particles (see Ref. [2] for a recent review emphasizing different examples such as gravitation, plasmas, fluid

* Corresponding author. Fax: +39-055-4796342.
E-mail address: ruffo@avanzi.de.unifi.it (S. Ruffo).
[1] Also at INFN Sezione di Firenze.

1007-5704/03/$ - see front matter
doi:10.1016/S1007-5704(03)00055-8

mechanics,...). Relevant physical examples displaying such anomalies are known in Newtonian gravity but also in plasma physics (although in the latter case the screening of attractive and repulsive Coulomb interactions may mitigate them).

As usual in theoretical physics, the study of simple toy models proves to be of major importance to attack more complex and realistic systems. In particular, simple mean-field models with infinite-range interactions turned out to be extremely useful. In spite of the fact that they are constantly used in statistical mechanics to describe cooperative phenomena, it is somehow singular that violation of additivity has hardly been recognized in the past. A reason for that lies perhaps in the fact that the thermodynamic limit is performed resorting to saddle-point techniques, which puts the Hamiltonian in the explicitly decoupled form, thus hiding the difficulties inherent in the long-range interaction. Indeed, ensemble inequivalence (for example between microcanonical and canonical ensemble) has been observed, producing effects like negative specific heats, which are the counterparts of the ones known in the gravitational context [1].

The advantage of such models is that their canonical thermodynamics can be exactly derived by performing the mean-field limit (the infinite N limit at fixed volume), which is a reasonable surrogate of the thermodynamic limit (the infinite N limit at fixed density). Contrary to the usual belief, an exact microcanonical solution is also feasible for such nontrivial Hamiltonians, using large deviations techniques [3], but the results will be presented elsewhere [4]. Here, for what concerns the microcanonical ensemble, we will mainly limit ourselves to show the result of numerical simulations, which, because of the mean-field nature of the interaction, require *only* $\mathcal{O}(N)$ codes (instead of the usual $\mathcal{O}(N^2)$). Moreover, further insight can be gained from solving the one-dimensional collisionless Boltzmann-Poisson equation for the single-particle distribution function, which becomes exact in the $N \to \infty$ limit (at all finite times) [5].

In the present paper, we investigate, both analytically and numerically, two simple mean-field models which we denote as "ϕ^4" and "ϕ^6", which display respectively second (ϕ^4) and first and second-order phase transitions separated by tricritical points (ϕ^6) in the canonical ensemble. Of the former model, we investigate in addition the dynamical formation of clustered states at low temperatures and we study their destabilization. The presence of quasi-stationary out-of-equilibrium states is moreover revealed close to the second-order phase transition, in analogy with what is found for the Hamiltonian mean-field (HMF) model (see [6] for a recent review). Concerning the ϕ^6-model, we study the phase diagram in the canonical ensemble and we report numerical simulations of hysteretic effects near first-order phase transitions. We point out the existence of a narrow region of negative specific heat.

2. The mean-field ϕ^4 model

Let us first consider the following Hamiltonian:

$$H = \sum_{i=1}^{N} \left[\frac{p_i^2}{2} - (1-\theta)\frac{q_i^2}{2} + \frac{q_i^4}{4} \right] - \frac{\theta}{2N} \sum_{i,j=1}^{N} q_i q_j, \tag{1}$$

where p_i is the conjugate momentum of the variable q_i, which defines the position of the ith particle on a line. This is a mean-field model since all particles are connected to all others, and the summation in the last term is *not* restricted to neighboring particles. Notice that positive (resp.

negative) values of the parameter θ correspond to attractive (resp. repulsive) mean-field interactions. All variables are dimensional and, for the sake of comparison, we have used the same parametrization introduced in Ref. [7] (which can be shown to be minimal by conveniently rescaling the variables and time). The local potential displays a double well for $\theta < 1$ and a single well otherwise. The ground-state energy per particle is $e_0 = -1/4$ for positive θ (all particles in a single cluster) and $e_0 = -1/4 + \theta/2$ in the repulsive case (double cluster).

2.1. Dynamics of the magnetization: the generation of clusters

Introducing the time-dependent magnetization

$$M = \frac{1}{N}\sum_{i=1}^{N} q_i, \tag{2}$$

we are therefore interested in the following equations of motion:

$$\ddot{q}_i = (1-\theta)q_i - q_i^3 + \theta M. \tag{3}$$

We study the dynamics of particle released with a water bag [8] initial condition where positions and momenta are uniformly distributed at random in the intervals $[q_0 - w_q/2, q_0 + w_q/2]$ and $[-w_p/2, +w_p/2]$, respectively. We have adopted the symplectic sixth-order Yoshida's algorithm [9], with a time step $\mathrm{d}t = 0.05$, which allows us to obtain an energy conservation with a relative accuracy $\Delta E/E$ ranging from 10^{-7} to 10^{-10}.

Fig. 1 shows the result: a coherent oscillating cluster self-consistently moving in the self-generated potential. The data are obtained for an initial condition with a small velocity dispersion,

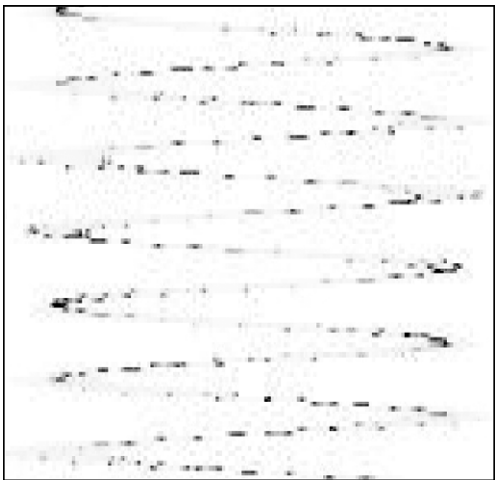

Fig. 1. Dynamics of the cluster. Evolution of the density $\rho(q)$ of formula (5) in grey scale for short times. The darker the grey, the bigger the density. Space is horizontal, thereas the vertical downward direction corresponds to time. One notices the periodic motion with the characteristic time scale ω_M^{-1}, defined in the text. In this simulation $N = 4096$, $\theta = 0.5$.

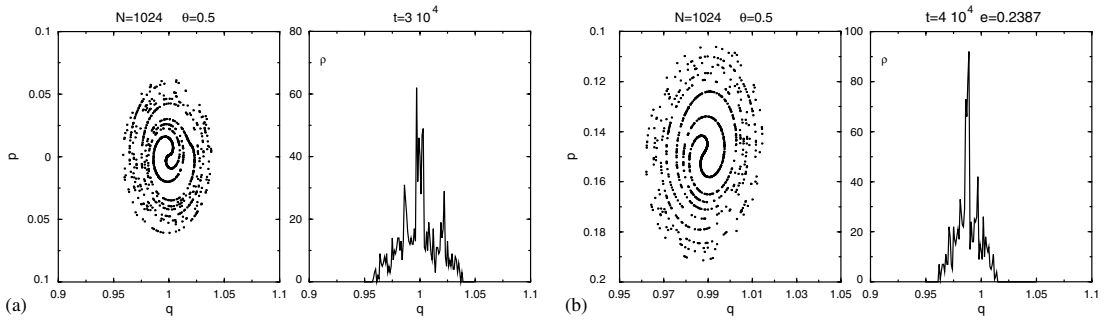

Fig. 2. Phase space snapshots of the cluster and the corresponding density $\rho(q)$ of formula (5) at two different times. In this simulation $N = 1024$, $e = -0.2387$, $\theta = 0.5$.

i.e. $q_0 = 1.1$, $w_q = 0.05$, $w_p = 0.0001$. Besides the oscillation of the center, the particles display a rotating motion around it, which creates a spiral structure (see Fig. 2), as frequently encountered in long range systems; we have found this coherent behavior for a very large collection of initial states. Notice that the spiral structure in the center is responsible for the very large peaks in the single particle density (right panels in Fig. 2). A similar phenomenon has been described successfully for the antiferromagnetic HMF model in terms of shock waves [10,11] by considering the associated Vlasov equation valid in the $N \to \infty$ limit.

We will therefore rely on a Vlasov-like approach. Denoting by $f(q,p,t)$ the one particle distribution function, we have here

$$\frac{\partial f}{\partial t} + p\frac{\partial f}{\partial q} + \frac{\partial f}{\partial p}\left[(1-\theta)q - q^3 + \int_{-\infty}^{+\infty} \mathrm{d}u \int_{-\infty}^{+\infty} \mathrm{d}\alpha f(\alpha,u,t)\alpha\right] = 0. \tag{4}$$

Introducing a density field ρ and a velocity field v, as follows

$$\rho(q,t) = \int_{-\infty}^{+\infty} f(q,p,t)\,\mathrm{d}p \tag{5}$$

$$\rho(q,t)v(q,t) = \int_{-\infty}^{+\infty} pf(q,p,t)\,\mathrm{d}p \tag{6}$$

and neglecting velocity dispersion, we have recently shown [10] how to reduce this problem to appropriate hydrodynamical equations. A short-time analysis, performed for the HMF model, led us finally to a *dissipativeless* spatially forced Burgers equation. We expect that a similar treatment can be developed for the current model and that similar techniques could be applied. A well known property of the Burgers equation without viscosity, is that the solution becomes multi-stream after a *finite* time: the appearance of shock waves in the velocity profile corresponds indeed to singular points in the density profile (see Fig. 2). In the original *discrete* model, this phenomenon would correspond to particle crossing; after some time, fast particles will eventually catch slow ones downstream creating the so-called spiral dynamics exemplified in the left panels of Fig. 2.

2.2. Stability analysis

To understand the origin of this cluster and its stability, we will first consider the simplest case of a fully clustered state where $q_i = M$. In this simple case, the collective motion is ruled by the equation

$$\ddot{M} = M - M^3, \tag{7}$$

which can be easily solved using elliptic functions [12]. Integrating Eq. (7), between the initial time, when the cluster is released without kinetic energy at the position $q = a > 1$, and time t, we get

$$M = a\,dn\left(\frac{at}{\sqrt{2}}, k\right), \tag{8}$$

where dn is the elliptic delta amplitude function and $k = (2 - 2/a^2)^{1/2}$ the modulus of Jacobi elliptic functions. We remind that this solution is periodic, with the amplitude-dependent period given in terms of the complete elliptic integral of the first kind $2K(k)$; the magnetization M will thus oscillate with a frequency $\omega_M = \pi a/\sqrt{2}K$, which will be the main timescale of the problem. One notices immediately that the modulus k and the frequency ω_M are both functions of the same parameter, namely the amplitude a, related to the energy per particle $e = E/N$ through the relation $a^2 = 1 + (1 + 4e)^{1/2}$. This solution is interesting in its own, since explicit analytical solutions are not common for nonlinear nonintegrable systems of oscillators, but one should of course study its stability in order to understand why this coherent oscillating cluster emerges spontaneously. Using the equations of motion (3) for the q_i and introducing $\xi_i = q_i - M$, we obtain up to first-order

$$\ddot{\xi}_i + (\theta - 1 + 3M^2)\xi_i = 0. \tag{9}$$

Introducing the new variable $u = at/\sqrt{2}$, we obtain the Lamé equation in its canonical form

$$\frac{\mathrm{d}^2\xi_i}{\mathrm{d}u^2} + [\alpha - v(v+1)k^2\mathrm{sn}^2(u,k)]\xi_i = 0, \tag{10}$$

with $\alpha = 6 + 2(\theta - 1)/a^2$ and $v = 2$. For integer values of v, many rigorous results are known [13,14] and in particular it is established that there are only $v + 1$ instability regions in the (α, k) plane. The stability charts could be explicitly constructed [15] by observing that Eq. (10) has the following five periodic solutions:

$$y = 1 - \frac{\alpha}{2}\mathrm{sn}^2(u,k) \quad \text{with } \alpha = 2[1 + k^2 \pm (k^4 - k^2 + 1)^{1/2}], \tag{11}$$

$$y = \mathrm{cn}(u,k)\mathrm{d}n(u,k) \quad \text{with } \alpha = 1 + k^2, \tag{12}$$

$$y = \mathrm{sn}(u,k)\mathrm{d}n(u,k) \quad \text{with } \alpha = 1 + 4k^2, \tag{13}$$

$$y = \mathrm{sn}(u,k)\mathrm{cn}(u,k) \quad \text{with } \alpha = 4 + k^2. \tag{14}$$

Thus the above curves $\alpha = \alpha(k^2)$ define the boundary curves of the three $(v + 1)$ nondegenerate instability regions. Theses curves are presented in the plane (θ, e) in Fig. 3.

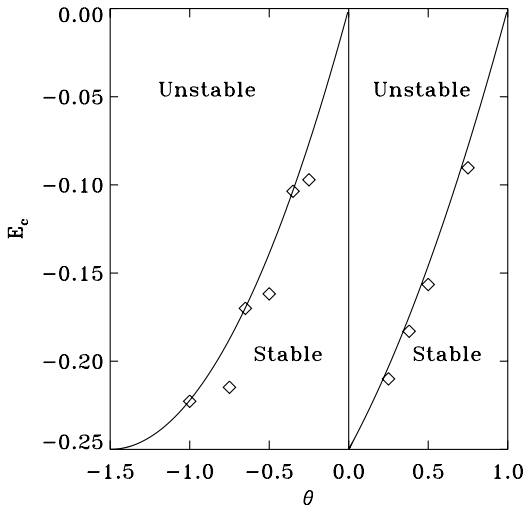

Fig. 3. Critical energy as a function of the parameter θ. The solid line corresponds to the results given by the stability charts derived analytically (or, alternatively, using the Floquet analysis), whereas the diamonds correspond to the results of microcanonical simulations for an ensemble of $N = 1024$ particles.

One can also investigate the linear stability of this cluster solution with a standard Floquet analysis, i.e. computing the eigenvalues of the $2N \times 2N$ matrix of the tangent map. Here, contrary to usual lattice systems with coupling between neighbors, Eq. (9) shows that we obtain N identical second-order equations; this is a direct consequence of the mean-field character of Hamiltonian (1). Consequently, we obtain two different N times degenerate Floquet eigenvalues and the periodic solution is linearly stable when the eigenvalues lie on the unit circle in the complex plane.

At this stage, one derives numerically the linear stability threshold by considering the numerical evolution of two different initial conditions (1,0) and (0,1) for the vector $(\xi, \dot{\xi})$. The dynamics is solved by a standard fourth-order Runge–Kutta algorithm for the time integration of Eq. (9), where the magnetization M is either directly integrated using Eq. (7) or implemented with the help of Eq. (8). For a given value of θ, an energy threshold exists, above which the largest Floquet multiplier is greater than unity, and therefore the solution is unstable. The solid line in Fig. 3 shows the evolution of this threshold as a function of the parameter θ. The analytical calculations were directly compared with the numerical thresholds obtained by considering a water bag with very small but finite width, i.e. $w_q \ll q_0$ and $w_p \ll 1$, to make a direct comparison with the above analytical results. Checking on Fig. 3, one gets, apart from a slight underestimate, a good agreement between numerics and theory. It should however be remarked that, for the finite N systems, stability persists only for a finite time, which presumably diverges as N increases, as it happens for the HMF model [6,11].

2.3. Equilibrium statistical mechanics

The partition function can be computed by means of a standard Hubbard–Stratonovich transformation. Indeed, for a Hamiltonian of the general form

$$H = \sum_{i=1}^{N} \left[\frac{p_i^2}{2} + V(q_i) \right] - \frac{\theta}{2N} \left(\sum_{i=1}^{N} q_i \right)^2, \tag{15}$$

the partition function is

$$Z = \int_{-\infty}^{+\infty} \prod_{\ell=1}^{N} \mathrm{d}p_\ell \, \mathrm{d}q_\ell \, \mathrm{e}^{-\beta H} = Z_K Z_V = (2\pi/\beta)^{N/2} Z_V, \tag{16}$$

where the configurational partition function is

$$Z_V = \int_{-\infty}^{+\infty} \prod_{\ell=1}^{N} \mathrm{d}q_\ell \, \mathrm{e}^{-\beta V(q_\ell)} \, \mathrm{e}^{\frac{\beta\theta}{2N}\left(\sum_{i=1}^{N} q_i\right)^2}. \tag{17}$$

We use at this point the Hubbard–Stratonovich trick, i.e. we consider the identity

$$\mathrm{e}^{\mu x^2} = \frac{1}{\sqrt{\pi}} \int_{-\infty}^{+\infty} \mathrm{d}y \, \mathrm{e}^{-y^2 + 2\sqrt{\mu} x y}. \tag{18}$$

Defining

$$\psi(x, \beta) = \ln \left[\int_{-\infty}^{+\infty} \mathrm{d}q \, \mathrm{e}^{-\beta V(q) + xq} \right], \tag{19}$$

after some algebra one gets

$$Z_V = \sqrt{\frac{N}{2\beta\theta\pi}} \int_{-\infty}^{+\infty} \mathrm{d}x \, \mathrm{e}^{-N\beta f_{\mathrm{L}}(x,\beta)} \tag{20}$$

$$\beta f_{\mathrm{L}} = \frac{x^2}{2\beta\theta} - \psi(x, \beta) \tag{21}$$

where f_{L} is the configurational Landau free energy. In the thermodynamic limit, one can evaluate the above integral by means of the saddle point approximation. The saddle point is determined by the condition $\bar{x} = \beta\theta\psi_x(\bar{x}, \beta)$, (where ψ_x denotes the derivative with respect to x) and can be evaluated numerically in a self-consistent manner. Notice that $\bar{x} = 0$ is always a solution if the potential V is even.

Finally, we can thus express the configurational partition function as

$$Z_V = \frac{1}{\sqrt{\beta\theta\psi_{xx}(\bar{x}, \beta) - 1}} \exp \left[N \left(\psi(\bar{x}, \beta) - \frac{\bar{x}^2}{2\beta\theta} \right) \right]. \tag{22}$$

Up to terms of order $\mathcal{O}(1/N)$, the relevant equilibrium observables can be expressed accordingly as a function of $\bar{x}$, using the following formulæ:

$$\beta f = -\frac{1}{N} \ln Z = -\frac{1}{2} \ln(2\pi/\beta) - \psi(\bar{x}, \beta) + \frac{\bar{x}^2}{2\beta\theta} \tag{23}$$

$$M = \left\langle \frac{1}{N} \sum_{i=1}^{N} q_i \right\rangle = \frac{\bar{x}}{\beta\theta} \tag{24}$$

$$e = \frac{\partial \beta f}{\partial \beta} = \frac{1}{2\beta} - \psi_\beta(\bar{x}, \beta) - \frac{\bar{x}^2}{2\beta^2\theta} = \frac{1}{2\beta} - \psi_\beta(\bar{x}, \beta) - \frac{\theta}{2} M^2. \tag{25}$$

In the disordered phase, when $M = 0$, the system reduces to an ensemble of independent anharmonic oscillators. In the ferromagnetic case ($\theta > 0$), as presented in Fig. 4, the model displays a second-order transition in the canonical ensemble, in full agreement with previous results based on the Fokker-Planck approach [7]. The magnetization vanishes as $(T_c - T)^{1/2}$ in the subcritical regime and the specific heat has a finite jump at T_c. Conversely, in the antiferromagnetic case ($\theta < 0$), no transition occurs, and $\bar{x} = 0$ is the only solution of the consistency equation for any value of the temperature. The free energy and the internal energy are always given by the above formulæ, with zero magnetization.

As this behavior is clearly reminiscent of the HMF model, that we have already studied in the past [10,16,17], and where the presence of long-lived out-of-equilibrium states was surprisingly discovered, it was natural to suspect that they also appear in the present model. We have therefore performed two types of numerical simulations: microcanonical ones with a symplectic algorithm (sixth-order Yoshida or fourth-order McLachlan-Atela [18]) and canonical ones with a Nosé-Hoover thermostat [19] (fourth-order Runge–Kutta algorithm). No appreciable deviations are observed between the two types of simulations for initial conditions close to equilibrium, see Fig. 4.

However, a region with clear differences is found for "water-bag" initial conditions: see an example for $q_0 = 0$ in Fig. 5. This is strongly reminiscent of similar observations made on the HMF model [16,20]. The fact that some points lie on the branch with vanishing magnetization also in the subcritical region (see Fig. 5b) indicates that this is a metastable state in the micro-

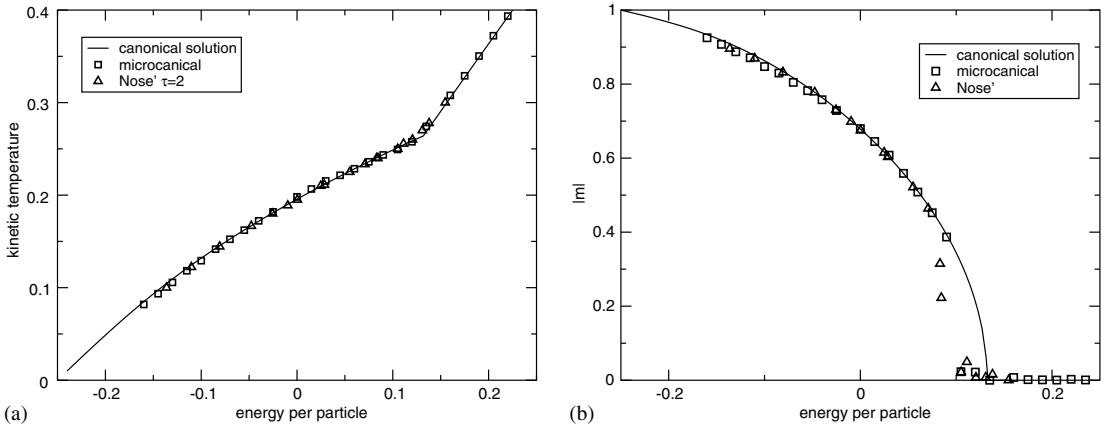

Fig. 4. Comparison of ensembles for the ϕ^4 model, $\theta = 0.5$, $N = 512$: caloric (panel a) curve and magnetization (panel b). Squares and triangles refer to microcanonical and canonical simulations, respectively, while the solid lines are the exact canonical solutions given by Eqs. (25) and (24). The critical point is located at $T_c = 0.264$ ($e_c = 0.132$). In both cases the initial conditions were $q_i(0) = 1$ and $p_i(0)$ chosen randomly with a Gaussian distribution.

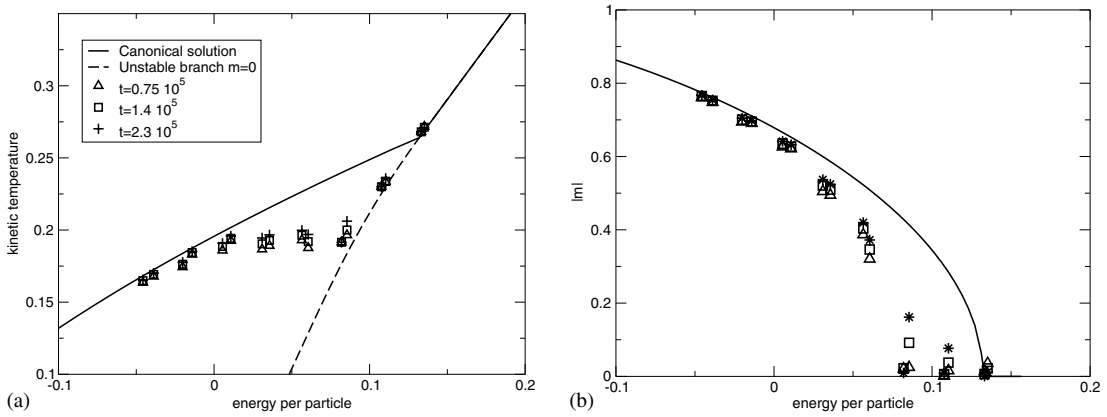

Fig. 5. Microcanonical results obtained using molecular dynamics simulations for the ferromagnetic ϕ^4 model: $\theta = 0.5$, $N = 10^4$ and water bag initial conditions $q_0 = 1$, $w_q = 10^{-4}$.

canonical ensemble. On the contrary, let us notice that triangles below the theoretical curve in Fig. 4b are due to finite size effects and would disappear for larger N values. A careful study of the numerical results for very large integration times shows a systematic tendency of these points to converge towards the equilibrium state indicated in Fig. 4 by the solid line. This attests the metastable character of these states.

Series of microcanonical runs for the repulsive case have shown that metastable states may possibly exist also in this case, and we suspect that they may be related to the existence of a stable cluster in the energy region $-1/4 < e \lesssim -0.097$. This metastability is thus of dynamical rather than of thermodynamical origin.

Summarizing, the ϕ^4 model has emphasized the striking appearence of a cluster and also dynamical differences between microcanonical and canonical ensembles, presumably related to slow relaxation towards the final Boltzmann–Gibbs equilibrium state; ensemble inequivalence appears only in a transient. Indeed, it has been recently reported in spin systems [21], that true ensemble inequivalence occurs in regions of first-order phase transitions. It would be therefore very interesting to exhibit a *dynamical* mean-field model of the polynomial class with a first-order phase transition. This is the purpose of the next section.

3. The mean-field ϕ^6 model

The simplest generalization of the previous model is

$$H = \sum_{i=1}^{N} \left[\frac{p_i^2}{2} + r\frac{q_i^2}{2} - \frac{q_i^4}{4} + \frac{q_i^6}{6} \right] - \frac{D}{2N} \sum_{i,j=1}^{N} q_i q_j, \tag{26}$$

where D and r are two independent parameters (also in this case it can be shown that this parametrization is minimal). The main interest of model (26) lies in the fact that it may exhibit a first-order phase transition for a proper choice of the parameters, and therefore possibly ensemble

inequivalence. This can be realized by first considering the zero temperature limit, where equilibrium states are given by the minima of the function

$$V_{\text{eff}} = \frac{r-D}{2}x^2 - \frac{x^4}{4} + \frac{x^6}{6}. \tag{27}$$

For $0 < r - D < 1/4$, such polynomial admits three minima located at $x = 0$ and $x = \pm x_+$ and two maxima at $x = \pm x_-$ where

$$x_\pm^2 = \frac{1}{2} \pm \frac{1}{2}\sqrt{1-4(r-D)}. \tag{28}$$

A first-order transition can thus be expected within this parameter region. Furthermore, in order to have a first-order phase transition at $T = 0$ we must impose that the two minima attain the same value (equal to zero). This conditions holds for $r - D = 3/16$ and we can at least hope that close to this parameter values the transition persists also at nonzero temperature. We checked that this is indeed the case by computing the free energy in a self-consistent way, as explained in the previous section. The transition exists in a very narrow region *below* $r - D = 3/16$.

It is useful to consider the expansion up to sixth-order of the Landau free energy of the ϕ^6-model in order to determine the critical line of second-order transitions and the tricritical point. We obtain

$$\beta f_{\text{L}}(x,\beta) = \frac{x^2}{2\beta D} - \psi(x,\beta) = \text{const.} + \frac{ax^2}{2} + \frac{bx^4}{4} + \frac{cx^6}{6} + \mathcal{O}(x^8), \tag{29}$$

where

$$a(\beta, r, D) = \frac{1}{\beta D} - \langle q^2 \rangle, \tag{30}$$

$$b(\beta, r, D) = -\frac{(\langle q^4 \rangle - 3\langle q^2 \rangle^2)}{6}, \tag{31}$$

with

$$\langle q^m \rangle = \frac{\int q^m \mathrm{e}^{-\beta V(q)}\,\mathrm{d}q}{\int \mathrm{e}^{-\beta V(q)}\,\mathrm{d}q}. \tag{32}$$

The numerical solution of $a = 0$ yields the critical line of second-order transitions, see Fig. 6. The tricritical point, separating first and second-order phase transition, is determined by the more restrictive condition $a = b = 0$. Table 1 presents some values of the tricritical point as a function of the parameter D.

The canonical thermodynamics in the case of a first-order transition is further illustrated in Fig. 7. Three branches of solutions (two stable and one unstable) exist from $T = 0$ up to $T = T'$ where a saddle-node bifurcation occurs. The $m = 0$ branch is stable at all temperatures, while the stable (upper branch in Fig. 7) and unstable (lower branch in Fig. 7) $m \neq 0$ solutions meet and collide at $T = T'$. Notice that this is at variance with the Blume–Emery–Griffiths model [21] (BEG), where the three branches do not extend down to zero temperature.

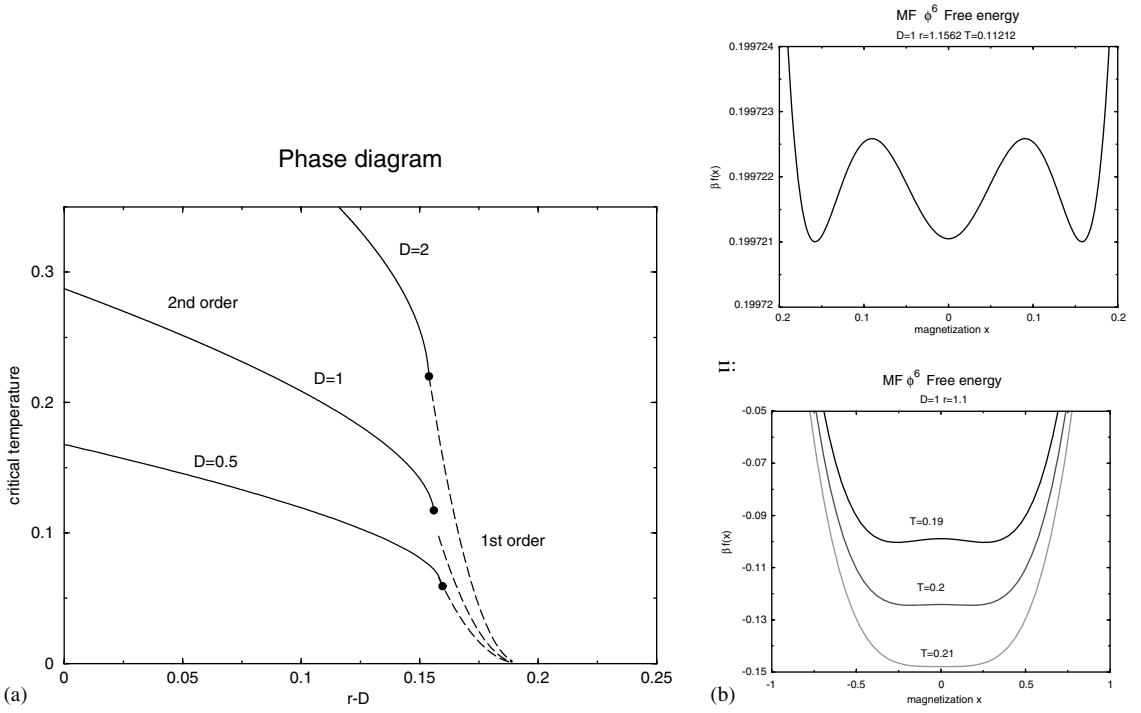

Fig. 6. Panel (a) shows the phase diagram of the ϕ^6 model for different values of the coupling constant D. The solid (respectively dashed) line marks the second (resp. first) order critical line, and the full dots the tricritical points. Panels (b) present the Landau free energy at a first-order transition close to the tricritical point $T_{\rm tr}$ and at a second-order transition occurring on the line $a = 0$, $T_{\rm c} = 0.205$.

Table 1
Some numerical values of the tricritical points of the ϕ^6 model. Notice that $T_{\rm tr}$ is approximatively proportional to the coupling constant D

D	$r - D$	T_{tr}
0.5	0.15965	0.05926
1	0.156068	0.115159
2	0.15393	0.22018
5	0.15247	0.52811

We have performed some simulations in the canonical ensemble to check this caloric curve. The results are in agreement with the theory and, as expected, display a marked metastability around the transition point (hysteretic effects). More specifically, three different initial conditions were adopted: (i) all $q_i = 0$; (ii) all $q_i = x_+$ and (iii) random distribution between $q_i = 0$ and $q_i = x_+$. In all cases, the p_i were initially chosen according to a random Gaussian distribution. Some microcanonical data are reported in Fig. 7 for an initial condition of type (ii).

A peculiarity of this model appears in some region of the parameters, when one considers the caloric curves. Indeed one notes in Fig. 7a that the $m = 0$ line (full) crosses the magnetized curve (dashed) to the left of T', the temperature corresponding to the saddle node bifurcation shown in

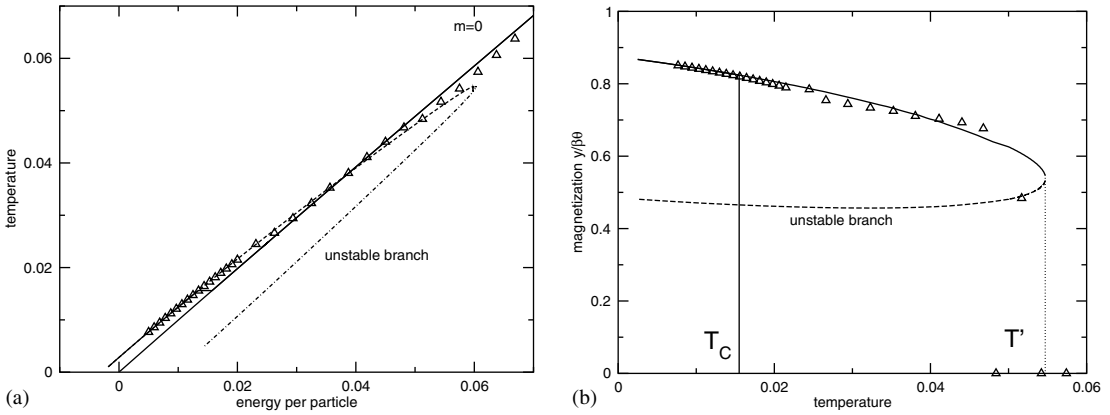

Fig. 7. Thermodynamics of the ϕ^6 model in the region of the first-order transition ($r = 1.18$, $D = 1.0$): Panel (a) presents the caloric curve and panel (b) the magnetization as a function of the energy. The critical temperature is $T_c = 0.0156 < T_{tr}$. Data obtained with microcanonical simulations, $N = 1024$ $t = 1.25 \times 10^6$.

Fig. 7b. This leads to the impossibility of applying the usual Maxwell construction. However, this is not always the case and, for example, $D = 1$, $r = 1.157 > r_{tr}$ leads to the usual features of a crossing to the right of T'. This confirms that in the interval $r \in [r_{tr}, 1.157]$, the mean-field ϕ^6 model has a narrow region of negative specific heat, where the transition will be first-order in the canonical ensemble and second-order in the microcanonical. Unfortunately, the points near T' are extremely difficult to obtain because of numerical inaccuracies, and we are therefore unable to report a clear determination of negative specific heat. In conclusion, this model shows a scenario similar to the BEG model [21], in the case of a *dynamical* Hamiltonian. Meanwhile, similar results have been published for some extensions of the HMF model [22].

4. Conclusion

The Blume–Emery–Griffiths mean-field model was shown to be an excellent benchmark to discuss relations between canonical and microcanonical ensembles in long range interacting systems [21]. Indeed, this model is exactly solvable in both ensembles and is, at the same time, sufficiently rich to display such interesting features as negative specific heat and temperature jumps in the microcanonical ensemble. However, it has no dynamics and only the thermodynamical behavior can be investigated. This is why we need to study models that displays all these interesting thermodynamical effects, but for which one would also dispose of an Hamiltonian dynamics. This point was already addressed in the framework of the HMF model and in particular in its two-dimensional version (see [6] for a review). Having access to dynamics, one can moreover study nonequilibrium features.

The mean-field models that we have considered in this paper are exactly solvable in the canonical ensemble by a Hubbard–Stratonovich transformation. The data in the microcanonical ensemble were obtained using molecular dynamics simulations. We have shown that these models have first and second-order phase transitions and tricritical points. Their phase diagram allows to

test the presence of ensemble inequivalence near canonical first-order phase transitions and we have also studied spontaneously generated out-of-equilibrium structures.

Acknowledgements

We would like to warmly thank Arkady Pikovsky and David Mukamel for the helpful discussions which are at the origin of this study. This work has been partially supported by EU contract no. HPRN-CT-1999-00163 (LOCNET network), the Pôle Scientifique de Modélisation Numérique de l'ÉNS Lyon, and the Région Rhône-Alpes through the *Bourse d'Acqueil* nr. 00815559. This work is also part of the contract COFIN00 on *Chaos and localization in classical and quantum mechanics*.

References

[1] Padmanabhan T. Statistical mechanics of gravitating systems. Phys Rep 1990;188:285.
[2] Dauxois T, Ruffo S, Arimondo E, Wilkens M, editors. Lecture notes in physics, vol. 602. Dynamics and thermodynamics of systems with long range interactions. Springer; 2002.
[3] Dembo A, Zeitouni O. Large deviation techniques and their applications. Springer-Verlag; 1998.
[4] Barré J, Bouchet F, Dauxois T, Ruffo S, in preparation.
[5] Spohn H. Large scale dynamics of interacting particles. Springer-Verlag; 1991.
[6] Dauxois T, Latora V, Rapisarda A, Ruffo S, Torcini A. Lecture notes in physics, vol. 602. The Hamiltonian mean field model: from dynamics to statistical mechanics and back. Springer; 2002.
[7] Desai RC, Zwanzig R. Statistical Mechanics of a nonlinear stochastic model. J Stat Phys 1978;19:1.
[8] Dawson JD. One-dimensional plasma model. Phys Fluid 1962;5:445;
Particle simulation of plasma. Rev Mod Phys 1983;55:403.
[9] Yoshida H. Constructions of higher order symplectic integrators. Phys Lett A 1990;150:262.
[10] Barré J, Bouchet F, Dauxois T, Ruffo S. Out-of-equilibrium states as statistical equilibria of an effective dynamics. Phys Rev Lett 2002;89:110601.
[11] Barré J, Bouchet F, Dauxois T, Ruffo S. Birth and long-time stabilization of out-of-equilibrium coherent structures. Eur Phys J B 2002;29:577.
[12] Lawden DF. Elliptic functions and applications. Springer; 1989.
[13] Whittaker ET, Watson GN. A course of modern analysis. fourth ed. Cambridge University Press; 1946.
[14] Arscott FM. Periodic differential equation. Oxford: Pergamon; 1964.
[15] Pecelli G, Thomas ED. An example of elliptic stability with large parameters Lamé's equation and the Arnold-Moser-Rüssmann criterion. Quart Appl Math 1978;36:129.
[16] Antoni M, Ruffo S. Clustering and relaxation in Hamiltonian long-range dynamics. Phys Rev E 1995;52:2361.
[17] Dauxois T, Holdsworth P, Ruffo S. Violation of ensemble equivalence in the antiferromagnetic mean-field XY model. Eur Phys J B 2000;16:659.
[18] MacLachlan RI, Atela P. The accuracy of symplectic integrators. Nonlinearity 1992;5:541.
[19] Nosé S. Unified formulation of the constant temperature molecular-dynamics methods. J Chem Phys 1984;81:511; Hoover WG. Canonical dynamics- Equilibrium phase-space distributions. Phys Rev A 1985;31:1695.
[20] Latora V, Rapisarda A, Tsallis C. Non-Gaussian equilibrium in a long-range Hamiltonian system. Phys Rev E 2001;64:056134.
[21] Barré J, Mukamel D, Ruffo S. Inequivalence of ensembles in a system with long-range interactions. Phys Rev Lett 2001;87:030601.
[22] Antoni M, Ruffo S, Torcini A. First and second order clustering transitions for a system with infinite-range attractive interactions. Phys Rev E Rapid Commun 2002;66:025103.